Bulletin of the Seismological Society of America, Vol. 82, No. 3, pp. 1453-1474, June 1992

NUMERICAL EXPERIMENTS IN BROADBAND RECEIVER FUNCTION ANALYSIS

BY J. F. CASSIDY*

ABSTRACT

The use of broadband receiver function analysis to estimate the fine-scale *S*-velocity structure of the lithosphere is becoming increasingly popular. A series of numerical experiments shows several important aspects of this technique, with emphasis on estimation of dipping interfaces. The recent modification introduced to the receiver function analysis technique that preserves absolute amplitudes (Ammon, 1991) is more robust than the previous technique of modeling receiver functions that were normalized to unit amplitude. Using the latter method, shallow (e.g., depths less than ~ 2 km) high-velocity contrast interfaces may alter the apparent amplitudes of *Ps* phases and produce inaccuracies in the Earth model developed. The use of absolute amplitudes minimizes this potential for error. When research targets include deep dipping structure, tight stacking bounds (e.g., ≦ 10° in backazimuth (BAZ) and epicentral distance (Δ)) should be applied to avoid attenuating *Ps* phases and to aid in the identification of reverberations or scattered energy. Reverberations sample a relatively large lateral range about the recording site (e.g., a radius of 1 to 1.5 times the depth of the reflecting interface) and in the presence of dipping interfaces exhibit drastic variations in amplitude and arrival time as a function of BAZ and Δ. Thus, they cannot readily be used to provide constraints on the Earth structure. Formal inversion techniques, which attempt to match all arrivals in the waveform, must be used with caution when modeling receiver functions from complex regions. Only those phases whose amplitude and arrival-time variations as a function of BAZ and Δ are consistent with those of *Ps* conversions should be modeled. Forward modeling may resolve, depending upon the data quality and noise level, *S*-velocity contrasts greater than ~ 0.2 to 0.4 km / sec. Layers of thickness 2 to 5 km may be accurately imaged, and transition zones may be examined by considering various frequency bands of the data. In order to better understand the resolving power of the data, the averaging functions associated with the receiver functions may be calculated from the observed data and, if desired, used in the forward modeling process.

INTRODUCTION

Teleseismic *P* waveforms recorded at a three-component seismic station contain a wealth of information on the earthquake source, the Earth structure in the vicinity of both the source and the receiver, and mantle propagation effects. Receiver function analysis models the *P*-to-*S* converted phases (*Ps*) and reverberations associated with boundaries beneath the recording site. For events more than 30° distant, *P* waves are steeply incident and dominate the vertical component of ground motion, whereas *Ps* are contained almost exclusively on the horizontal components of ground motion. The amplitude, arrival time, and

* Present address: Geophysics Division, Geological Survey of Canada, 1 Observatory Crescent, Ottawa, Ontario K1A 0Y3, Canada.

polarity of the locally generated *Ps* phases are sensitive to the *S*-velocity structure beneath the recording site.

Teleseismic *P* waveforms have been modeled to estimate Earth structure beneath recording sites since the mid-1960s (e.g., Phinney, 1964; Burdick and Langston, 1977; Langston, 1979). Most of these studies employed long-period data to constrain the gross crustal properties. With the advent of digital broadband data, Owens *et al.* (1984) developed a linearized time-domain inversion routine to use with receiver functions. This routine, which requires the assumption of homogeneous, horizontal layers, has been successfully used in numerous studies (e.g., Owens *et al.*, 1987) to determine fine-scale *S*-velocity structure (i.e., 1- to 2-km-thick layers) to upper-mantle depths. Gross lateral variations in the Earth structure about the recording site have been examined (e.g., Owens *et al.*, 1984) by analyzing receiver functions corresponding to different backazimuths and developing acceptable Earth models for each.

Recently, receiver function analysis of broadband and short-period data has been applied to more complex tectonic settings where the assumption of homogeneous, horizontal structure does not apply (Ammon, 1985; Owens *et al.*, 1988; Langston, 1989; Lapp *et al.*, 1990). Here, the amplitude and arrival time of *Ps* phases and reverberations associated with dipping interfaces vary as a function of backazimuth (BAZ) and epicentral distance (Δ). In addition, *P* waves, *Ps* conversions, and reverberations have an azimuth-dependent transverse component of motion. Owens *et al.* (1988) and Lapp *et al.* (1990) have modeled the azimuthal variations in the direct *Ps* conversions contained in radial receiver functions to constrain the geometry of the subducting Juan de Fuca plate beneath Washington state. However, most previous receiver function studies have normalized both the observed and the synthetic receiver functions to unit amplitude. Recently, Ammon (1991) introduced a modification to the deconvolution technique that preserves the absolute amplitude of receiver functions. He notes that this modification provides information that may be used to constrain the near-surface velocity structure.

In view of the increased interest in the application of receiver function analysis of broadband and short-period data to estimate the *S*-velocity structure in complex tectonic environments, and the recent modification to the technique introduced by Ammon (1991), this paper has four primary goals. First, the use of absolute amplitudes in constraining dipping interfaces and the near-surface velocity structure is examined. I demonstrate that the modification introduced by Ammon (1991) provides important information on dipping interfaces and is more robust than the technique of modeling normalized amplitudes. Second, I examine the factors that should be considered in estimating stacking bounds for use in a dipping layer environment. An example that illustrates the potential hazards in choosing stacking bounds that are too large is given. Third, to formally invert receiver functions one must have confidence in their ability to model each arrival contained in the waveform. As such, the stability and lateral sampling range of *Ps* phases and reverberations in the presence of dipping interfaces are examined. Some techniques that may be used to discriminate between direct *Ps* conversions and reverberations are presented. Finally, this paper summarizes the resolution capability of receiver functions. I examine the minimum detectable ΔV_s, the ability to differentiate velocity gradients from first-order velocity discontinuities, and the ability to resolve thin (1 to 5 km thick) layers.

Receiver Function Estimation

In estimating receiver functions, the deconvolution technique proposed by Langston (1979) is employed to suppress the earthquake source and path effects, thereby isolating the locally generated *Ps* phases and reverberations. This is accomplished by deconvolving the vertical component of ground motion (assumed dominated by source and path effects) from the horizontal components. The details of this method are outlined in Langston (1979), Owens *et al.* (1984), and Ammon (1991). In theory, the radial receiver function is given by

$$E_R(\omega) = \frac{D_R(\omega)}{D_Z(\omega)}, \tag{1}$$

where $D_R(\omega)$ and $D_Z(\omega)$ are the frequency-domain representation of the recorded radial and vertical ground motions, respectively. In practice, due to noise in the data and the band-limited nature of the signal, the water-level method of Clayton and Wiggins (1976) is used to stabilize the frequency-domain spectral division. Thus, the deconvolution is given by

$$\tilde{E}_R(\omega) = \frac{D_R(\omega)}{D_Z(\omega)} A(\omega), \tag{2}$$

where $\tilde{E}_R(\omega)$ is our estimate of the true receiver function $E_R(\omega)$, and $A(\omega)$ is the averaging or "blurring" function associated with the deconvolution and is given by

$$A(\omega) = \frac{D_Z(\omega)\bar{D}_Z(\omega)G(\omega)}{\phi(\omega)}, \tag{3}$$

where

$$G(\omega) = \exp\left(\frac{-\omega^2}{4a^2}\right) \tag{4}$$

and

$$\phi(\omega) = \max\{D_Z(\omega)\bar{D}_Z(\omega), c \cdot \max[D_Z(\omega)\bar{D}_Z(\omega)]\}, \tag{5}$$

c is the water-level parameter expressed as a fraction of the maximum vertical component power spectra, and a controls the width of the Gaussian filter used to remove high-frequency noise. For broadband teleseismic data, a values between 3 and 7 are appropriate. An a value of 3 removes frequencies greater than ~ 0.5 Hz; an a value of 7 removes frequencies greater than ~ 2 Hz. Lower a values (e.g., 1 to 3) may be used to examine the low-frequency (~ 0.1 to 0.5 Hz) components of the data.

The recent modification to the deconvolution technique introduced by Ammon (1991) requires that the averaging function, $A(\omega)$, be normalized to unit amplitude in the time domain. This procedure provides absolute amplitude receiver functions by preserving the ratio P_r/P_z, where P_r and P_z represent the amplitude of the radial and vertical components of the direct P wave, respectively.

Transformation back to the time domain provides the estimate of the radial receiver function $\tilde{E}_R(t)$. The transverse receiver function $\tilde{E}_T(t)$ is determined in the same way (substitute the subscript "T" for the subscript "R").

The arrival time of *Ps* is sensitive to the depth-velocity product (Ammon *et al.*, 1990), while the amplitude is dependent upon the magnitude of the *S*-velocity contrast at the boundary; the polarity indicates whether the impedance contrast is negative or positive. An example of three-component data, radial and transverse waveforms and the corresponding receiver functions are given in Figure 1. The signal prior to time $T = 0.0$ sec is noise. The arrival at $T = 0.0$ sec in the receiver functions represents the direct *P* wave; subsequent phases are locally generated *Ps* phases or reverberations. Note that the near-source depth phase *pP*, prominent on the vertical component of ground motion, is not present in the radial receiver function.

Synthetic Receiver Functions

Synthetic seismograms are generated using a three-dimensional raytracing code written by T. J. Owens and based on Langston (1977b). The Earth model is parameterized in terms of a series of constant velocity, planar, dipping layers over a half-space. The *P*- and *S*-wave velocities, density, strike and dip angles, and thickness are specified for each layer in the model. Synthetic vertical, radial, and transverse seismograms are generated by specifying a backazimuth and ray parameter (incidence angle) for the plane *P*-wave incident at the base of the model. In addition to the direct *P* arrival and *Ps* conversions, the synthetic seismograms may (at the modelers' discretion) include the free-surface multiples associated with each interface. Synthetic receiver functions are computed using the deconvolution procedure described above, on the synthetic responses.

Dipping Layer Effects on Receiver Functions

The effects of dipping layers on receiver functions have been examined by Langston (1977b, 1979), Owens and Crosson (1988), and Owens *et al.* (1988). However, in these studies receiver functions were normalized to unit amplitude. I re-examine this situation using absolute amplitude receiver functions.

Dipping layers affect receiver functions in three ways. Consider a simple two-layer over a half-space model with an east-dipping boundary (dip angle $\delta = 15°$) at 20 km depth and a horizontal boundary at 40 km depth (Fig. 2a). The *S*-velocity contrast is 0.87 km/sec for both interfaces. Figure 2b illustrates the radial and transverse receiver functions generated using this model. Clearly there are significant differences between *Ps* phases generated at the dipping boundary (phase D) and those generated at the horizontal boundary (phase H) as a function of backazimuth. The three dipping layer effects on absolute amplitude receiver functions are the following.

1. *Ps* amplitudes and arrival times vary as a function of both BAZ (Fig. 2b) and Δ (not shown). Incident *P* waves traveling updip (i.e., approaching from BAZ = 90° in this example) generate the largest and latest arriving *Ps* phases; waves traveling downdip (BAZ = 270°) generate the smallest and earliest arriving *Ps* phases. The arrival-time variations as a function of BAZ are more clearly illustrated later in this paper.

2. The amplitude of the direct *P* wave in the radial receiver function has an azimuthal dependence. This variation is most pronounced for steeply dipping interfaces (e.g., $\delta \geqq 30°$) or more gently dipping boundaries having a large ΔV_s.

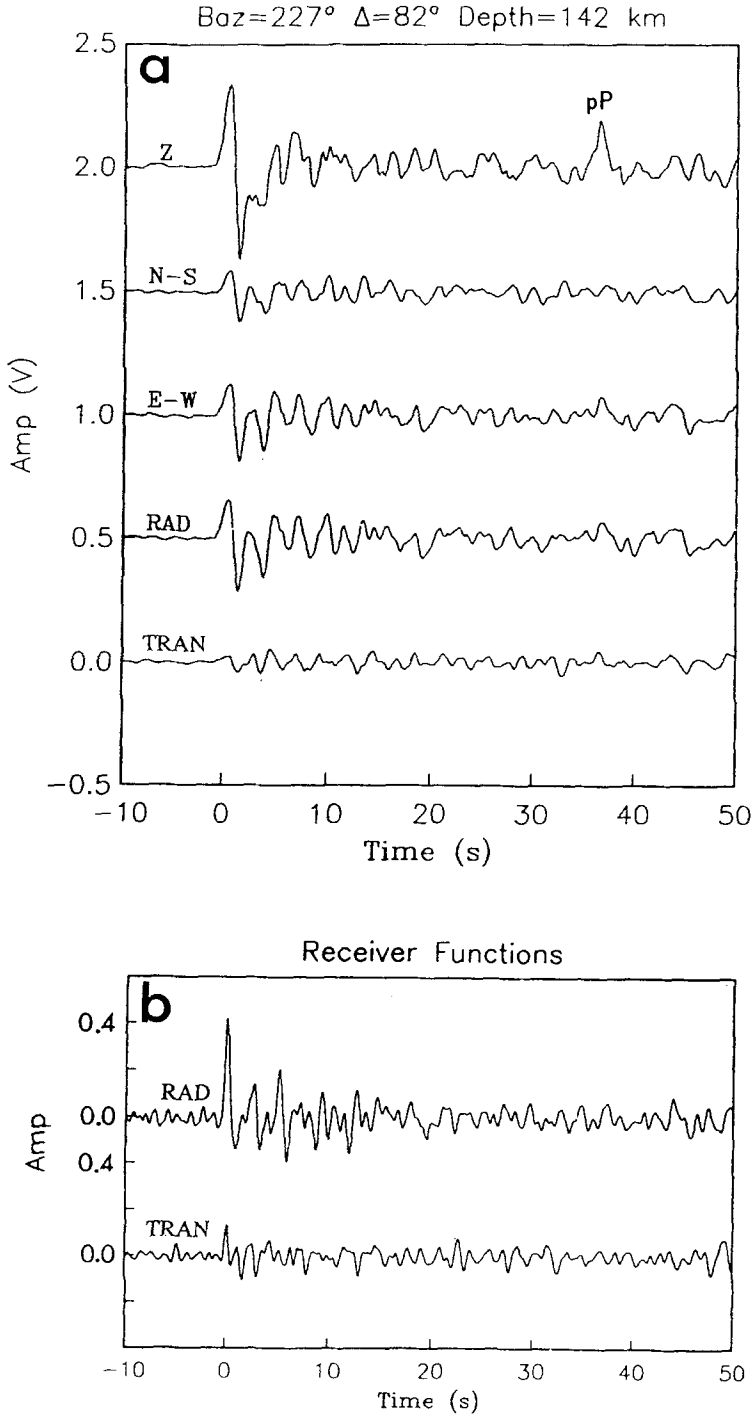

FIG. 1. (a) Three-component recordings (top three traces) and rotated horizontal components (lower two traces) of the 19 July 1988 $m_b = 6.0$ event in the Tonga Islands region (19.4°N, 175.2°W, O.T. = 01 00 20.5). These data were recorded at ALB-B on Vancouver Island (Cassidy, 1991). Z, N-S, and E-W represent the recorded vertical, north-south, and east-west components. "RAD" and "TRAN" represent radial and transverse waveforms obtained by rotating the horizontal components into the theoretical backazimuth of the ray. (b) Radial and transverse receiver functions were obtained by performing the deconvolution procedure described in text. The amplitudes are relative to the vertical component of the direct P wave.

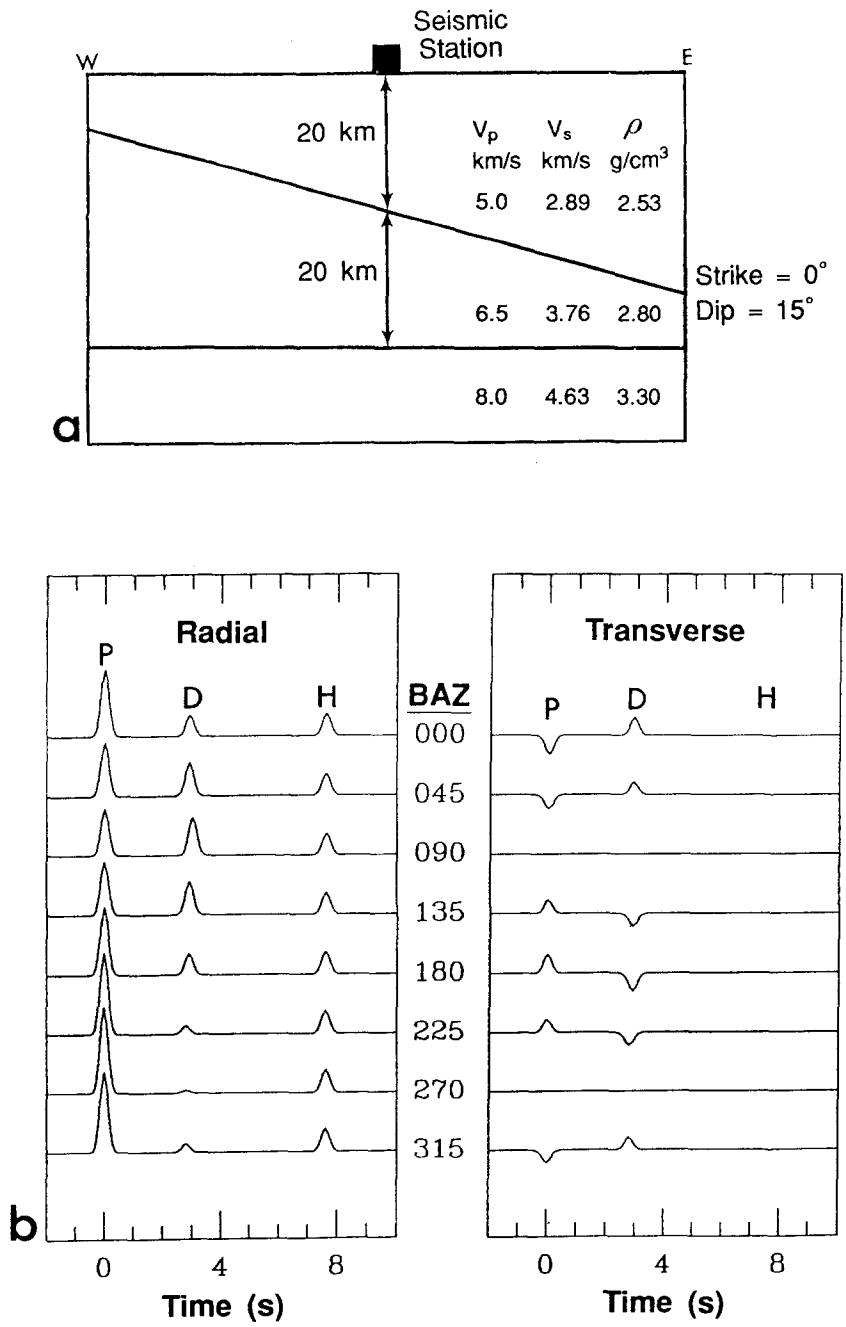

FIG. 2. (a) The Earth model used in this example. (b) Azimuthal variation in radial and transverse receiver functions resulting from a dipping interface (see text). P represents the direct *P* arrival; D and H denote *Ps* conversions from the eastward-dipping and the horizontal interface, respectively. Receiver functions were generated using a ray parameter of 0.068 sec/km (Δ = 45°).

Previous studies have normalized receiver functions to unit amplitude and therefore neglected this information, which is an immediate indicator of extreme structure beneath the recording site. As demonstrated in Figure 2b, the direct *P* wave in the radial receiver function is smallest for waves traveling

updip and largest for waves traveling downdip. However, if there are several interfaces dipping in different directions, a complex azimuthal amplitude pattern may result.

3. Dipping layers deflect P and S waves from the R-Z plane, thus introducing a transverse component of ground motion (Langston, 1977a). The transverse amplitude is zero for arrivals from the updip or downdip directions and largest for arrivals traveling along the strike direction of the interface (0° or 180° in this example). Note the transverse component of motion for both the direct P arrival (at $T = 0.0$ sec) and Ps generated at the dipping interface. Again, the presence of several interfaces dipping in different directions may result in a complex azimuthal amplitude pattern for the transverse component of the direct P wave. It is also noteworthy that the Ps phase generated at the horizontal boundary (phase H) is not significantly deflected off azimuth by the shallower, dipping interface.

Absolute versus Normalized Amplitudes

This section provides two examples, one for shallow structure and one for dipping structure, which illustrate the more robust nature of absolute amplitude receiver functions.

Shallow Structure. Most previous broadband receiver function studies have normalized radial and transverse receiver functions to unit amplitude, thereby neglecting the information provided by the ratio P_r/P_z. The modification to the deconvolution procedure recently introduced by Ammon (1991) preserves this ratio, which he notes is sensitive to the near-surface velocity structure.

To examine the effects of shallow structure on relative and absolute amplitude radial receiver functions, consider the two Earth models shown in Figure 3a. The only difference between these models is the 1.3-km-thick low-velocity (V_s = 1.73 km/sec) surface layer. Figure 3b compares the radial receiver functions normalized to unit amplitude for these two Earth models. To clearly illustrate the effects of shallow structure, only the direct P and Ps phases have been included in the synthetic waveforms shown. Tests made using the complete response do not alter the conclusion of this section. The low-velocity surface layer broadens the direct P arrival (i.e., the Ps phase generated at the base of this layer arrives shortly after the direct P wave and is not resolvable with this bandwidth) and results in an increase in the apparent amplitude (i.e., Ps/P_r) of the Ps phases. This is caused by refraction of the P and S waves towards the normal, which decreases the amplitude of P_r and increases the amplitude of Ps. If one were not aware of the surface layer when modeling, the large "apparent" Ps amplitude would lead to an overestimate of the ΔV_s for the boundaries at 10 and 30 km depth. In Figure 3c, the absolute amplitude receiver functions are compared for the two Earth models. In this case, the near-surface layer decreases the amplitude of the direct P arrival (P_r/P_z) but *does not alter* the amplitude of the Ps phases (Ps/P_z).

This example illustrates that, in the case of receiver functions normalized to unit amplitude, the amplitudes of Ps phases are sensitive not only to the ΔV_s of the generating boundary, but also to a certain extent on the shallow velocity structure. Given the subtle effect of the shallow structure (i.e., < 2 km depth) on the receiver function (i.e., the slight broadening of the direct P arrival), it may be difficult to identify or accurately model shallow boundaries. Reverberations may aid in the identification of these interfaces, however they are not

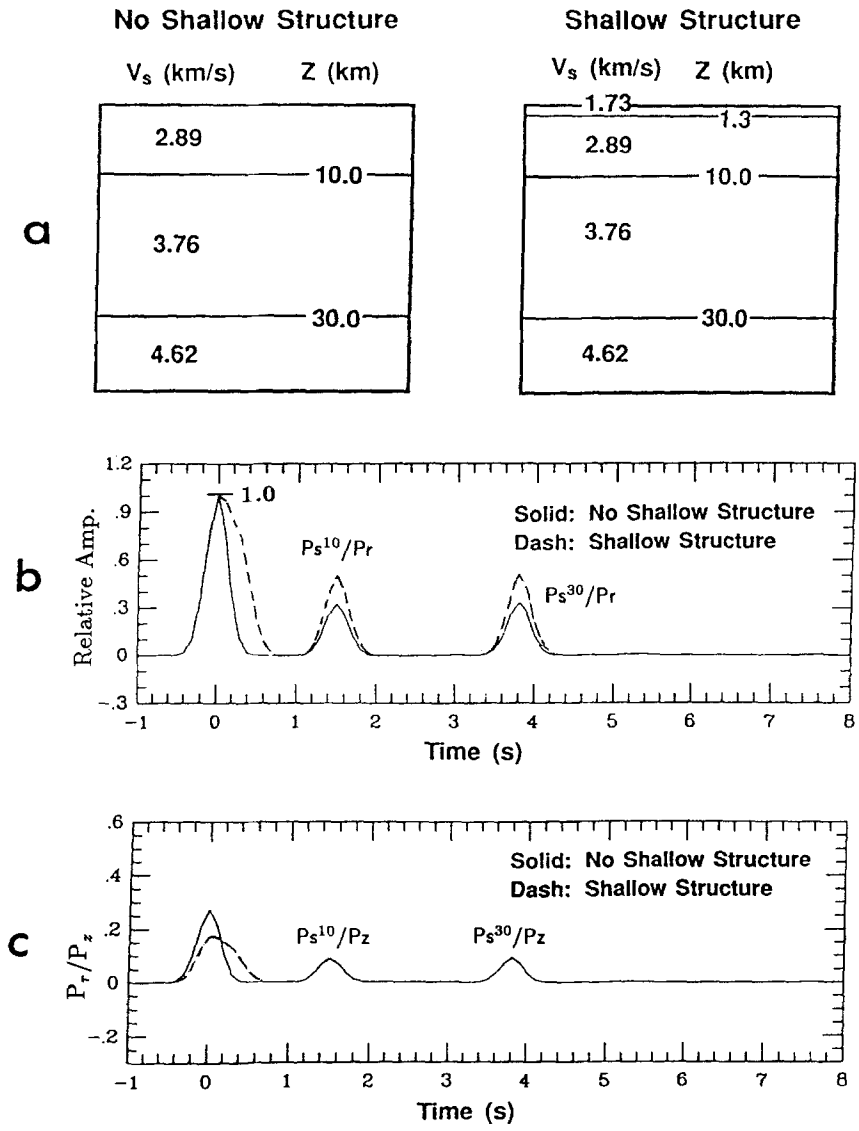

FIG. 3. Potential errors introduced by normalizing to unit amplitude in the presence of shallow structure. (a) Earth models used in this example. (b) Radial receiver functions normalized to unit amplitude. (c) Absolute amplitude radial receiver functions. If the shallow velocity structure is not resolved or is incorrectly modeled; normalizing to unit amplitude may alter Ps/P_r ratios and result in an incorrect earth model (see text).

always readily observed (e.g., see Owens and Crosson, 1988). Consequently, the ΔV_s of the deeper interfaces may not be accurately resolved. In contrast, *Ps* phases contained in absolute amplitude receiver functions are relatively insensitive to the shallow structure and allow an unambiguous determination of the ΔV_s across the generating boundaries. In addition, as pointed out by Ammon (1991), the absolute amplitude provides information on the shallow velocity structure. Figure 3c demonstrates that the low-velocity (V_s = 1.73 km/sec) near-surface layer may be recognized by the low P_r/P_z ratio of 0.16, compared to the value of 0.27 for the Earth model having a surface V_s of 2.89 km/sec.

Dipping Structure. Normalizing receiver functions to unit amplitude in a dipping layer environment may also result in inaccurate Earth models. Consider two simple Earth models. One is a two-layer reference model having a boundary (ΔV_s = 0.4 km/sec) dipping 15° to the east. The other is identical but, in addition to the above, has a shallower interface (ΔV_s = 0.25 km/sec) dipping 30° to the south. This boundary has a small enough ΔV_s that it may be difficult to resolve using receiver function analysis and must be considered a potential "missed boundary." First, we consider the case where the radial receiver function is normalized to unit amplitude. Figure 4a illustrates the amplitude ratio of *Ps* to the direct *P* wave (i.e., Ps/P_r) for the phase generated at the deeper east-dipping boundary as a function of BAZ for both the reference model and the more "complex" model. In this case, the largest Ps/P_r value does not correspond to the true dip direction of the deeper boundary (BAZ = 90°) but is offset by approximately 20°. In addition, the amplitude ratio is larger than expected from the reference model. If one were not aware of the shallow dipping boundary and modeled these data, both the dip direction and ΔV_s for the deeper boundary would be incorrectly estimated.

Figure 4b demonstrates that these potential modeling inaccuracies may be avoided by using absolute amplitudes. In this case, a potential "missed boundary" has no significant effect on the amplitude of a *Ps* phase generated at a deeper boundary.

Thus, the use of absolute amplitudes helps to avoid potential inaccuracies in Earth models for which shallow or dipping structure may be a factor.

Stacking Procedure

Receiver functions are generally stacked to enhance their signal-to-noise ratio (SNR) and suppress spurious arrivals. For receiver functions normalized to unit amplitude and study regions dominated by horizontal structure, Owens (1984) suggested stacking bounds of 20° in BAZ, and 10° (for the Δ range 45° to 60°) or 15° (over the Δ range 80° to 100°) in Δ.

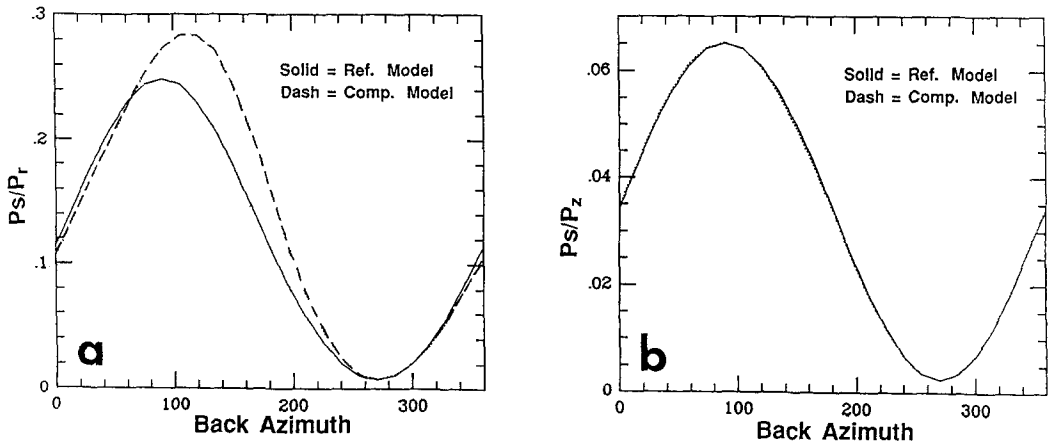

FIG. 4. Azimuthal amplitude variation of a *Ps* phase generated at an eastward-dipping boundary. The reference model (Ref.) contains only a single eastward-dipping interface; the more complex model (Comp.) is similar but also contains a shallower, southward-dipping interface (see text). (a) Normalizing to unit amplitude may result in an incorrect estimate for the dip direction and ΔV_s for the deeper boundary if the shallow boundary is not imaged. (b) The use of "absolute" amplitudes eliminates this potential for error.

Here, stacking bounds appropriate for use with absolute amplitude receiver functions in a dipping layer environment are examined. I do not attempt to derive strict stacking bounds, as this will depend upon the data set, but rather illustrate the factors that should be considered when stacking data, the potential hazards in choosing stacking bounds that are too large, and the advantages of using tight stacking bounds.

Ps phases generated at dipping interfaces exhibit amplitude and arrival-time variations as a function of both BAZ and Δ. The amplitude variation depends primarily upon the dip angle, whereas the arrival-time variation depends upon both the dip angle and the depth of the boundary. In general, *Ps* originating at greater depths will experience larger arrival-time variations for a given change in either BAZ or Δ. If the research targets include deep (e.g., 60 km depth) dipping interfaces, it is important to ensure that the stacking procedure employed to improve the SNR of the receiver functions does not diminish or significantly alter *Ps* conversions generated at those boundaries.

Figure 5 illustrates the amplitude and arrival-time variations as a function of BAZ and ray parameter (p) for a *Ps* phase generated at an eastward-dipping boundary ($\delta = 20°$) at 60 km depth (Table 1). The most rapid variation in both

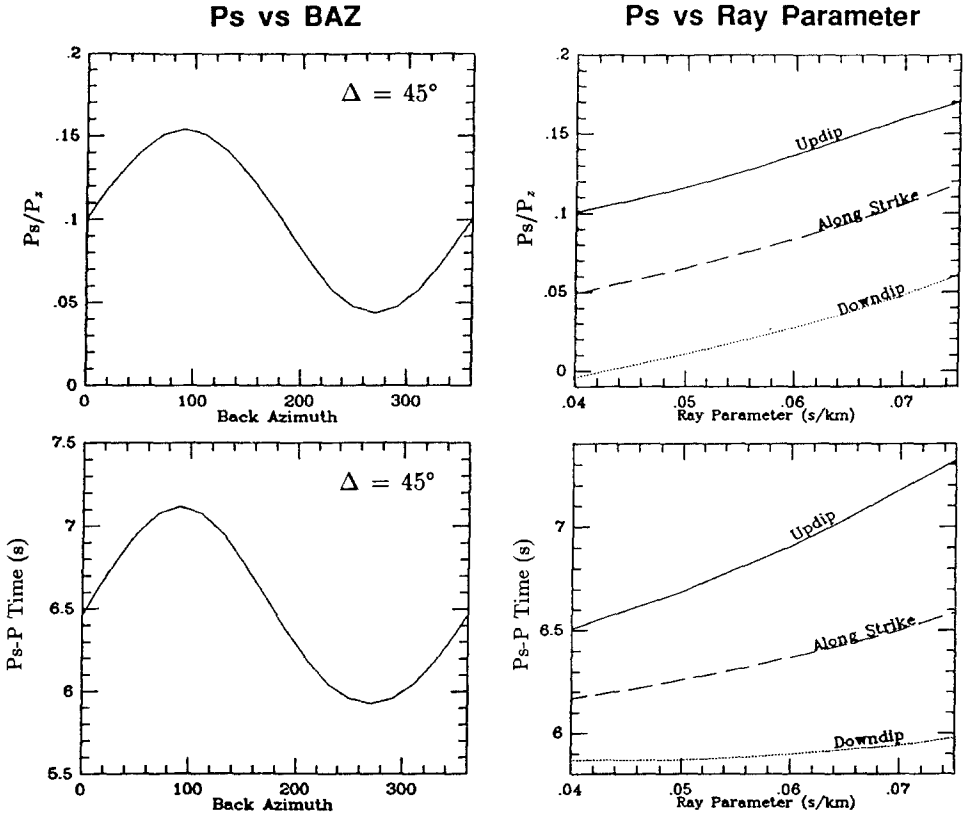

FIG. 5. Amplitude and arrival-time variation as a function of backazimuth and ray parameter for a *Ps* phase generated at a boundary at 60 km depth and dipping 20° to the east (see Table 1). Note that the most rapid azimuthal variations occur near the interface strike direction. Variations as a function of ray parameter (or Δ, see text) occur most rapidly for large values of the ray parameter (small Δ) and updip arrivals (i.e., waves traveling updip).

TABLE 1

REFERENCE MODEL USED FOR P_S STACKING TESTS

Layer No.	Vp (km/sec)	Vs (km/sec)	ρ (g/cm^3)	Thickness (km)	Dip Angle	Dip Direction
1	6.50	3.76	2.80	30	00	00
2	8.00	4.62	3.30	25	00	00
3	7.00	4.05	2.94	5	20	90
4	8.00	4.62	3.30	∞	20	90

the amplitude and arrival time of a *Ps* phase generated at a dipping interface occurs along the strike direction of the boundary. It is noted that arrival-time variations play a large role in the potential error introduced by stacking. For example for $p = 0.068$ ($\Delta = 45°$) the arrival time of the *Ps* generated at the boundary at 60 km depth varies by as much as 0.21 sec over a BAZ range of 20° (Fig. 5). For $p = 0.046$ ($\Delta = 80°$) the corresponding time shift is 0.13 sec. Thus, as pointed out by Owens (1984), tighter bounds should be applied to both BAZ and Δ when stacking events of $\Delta < 60°$. However, as demonstrated later in this section, there are advantages to stacking over the smallest possible range always.

Figure 6a demonstrates a potential hazard in choosing stacking bounds that are too large when attempting to resolve deep dipping structure. In this diagram, synthetic data using $a = 5$ (corresponding to frequency $\leqq 1$ Hz) are stacked over a range of 20° in BAZ and 10° in Δ. The top two traces represent synthetic receiver functions at the extremal bounds of both the BAZ and Δ range, and the third trace is the synthetic receiver function corresponding to the middle of the stacking range. The top two traces are stacked to form the lower-most trace, which ideally would be identical in appearance to the one immediately above it. Note that the direct *P* wave and the *Ps* phase generated at the horizontal boundary are not altered by stacking. However, the *Ps* generated at the dipping boundary at 60 km depth has been attenuated by 38%. If this exercise is repeated using tighter stacking bounds of 6° in BAZ and 5° in Δ (e.g., used in a recent study by Cassidy, 1991), the *Ps* phase generated at the 60-km-depth dipping interface is only attenuated by 6% (Fig. 6b).

This example, with only two events stacked from opposite bounds in both the BAZ and Δ range where amplitudes and arrival times vary most rapidly, demonstrates the potential hazards in using stacking bounds that are too large when one is interested in *Ps* phases generated at deep dipping boundaries. Stacking bounds should be examined for each study based on the research goals, the frequency content of the data, and the data distribution. The narrower width of higher-frequency receiver functions (e.g., $a = 5$ to 7) relative to lower-frequency receiver functions (e.g., $a = 1$ to 3) makes them more susceptible to error introduced by the arrival-time variations in *Ps* over BAZ and Δ ranges. Tighter stacking bounds should be applied when research goals include deep dipping interfaces, for data over the distance range $30° \leqq \Delta \leqq 60°$, and when using higher-frequency data (e.g., $a = 5$ to 7).

Stacking over a small range of BAZ and Δ is also advantageous, as it allows the identification of phases in receiver functions that vary rapidly in either amplitude or arrival time as a function of only slight changes in either BAZ or Δ. Such phases represent reverberations or scattered energy. A real data

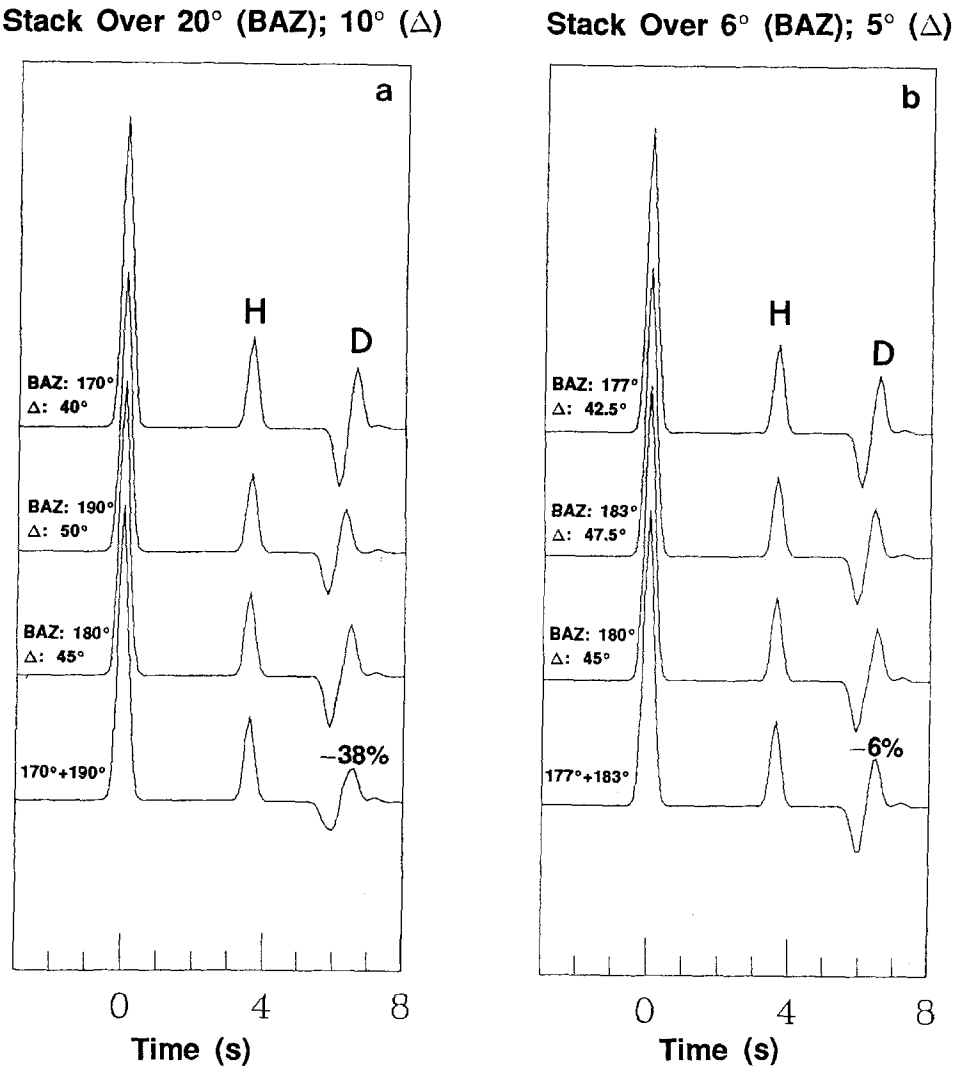

FIG. 6. Examples of stacking receiver functions generated using the model given in Table 1: over 20° in BAZ and 10° in Δ; and 6° in BAZ and 5° in Δ. In both cases, the lowermost trace represents the average of the top two traces and ideally would be identical to the trace immediately above it. Note that for *Ps* generated at a horizontal boundary (H) stacking over the larger bounds produces negligible error. However, in this example (see text), the amplitude of the *Ps* phase generated at the dipping interface at 60 km depth is reduced by 38% for the larger stacking bounds and only reduced by 6% for the smaller stacking bounds.

example is given in Figure 7, where the solid and dashed traces represent, respectively, stacks of eight radial receiver functions at $\Delta = 80°$ ($p = 0.046$) and four radial receiver functions at $\Delta = 90°$ ($p = 0.041$). The backazimuth for both stacks is 230°. Over this slight Δ range of 10° ($\Delta p = 0.005$ sec/km), the significant amplitude and arrival time variation of the two phases labeled "Reverb?" cannot be explained by *Ps* conversions generated at a planar dipping interface. These arrivals must therefore represent either reverberations or scattered energy and should not be quantitatively modeled. Another advantage of stacking within tight bounds is that it is easier to correlate arrivals from trace to trace.

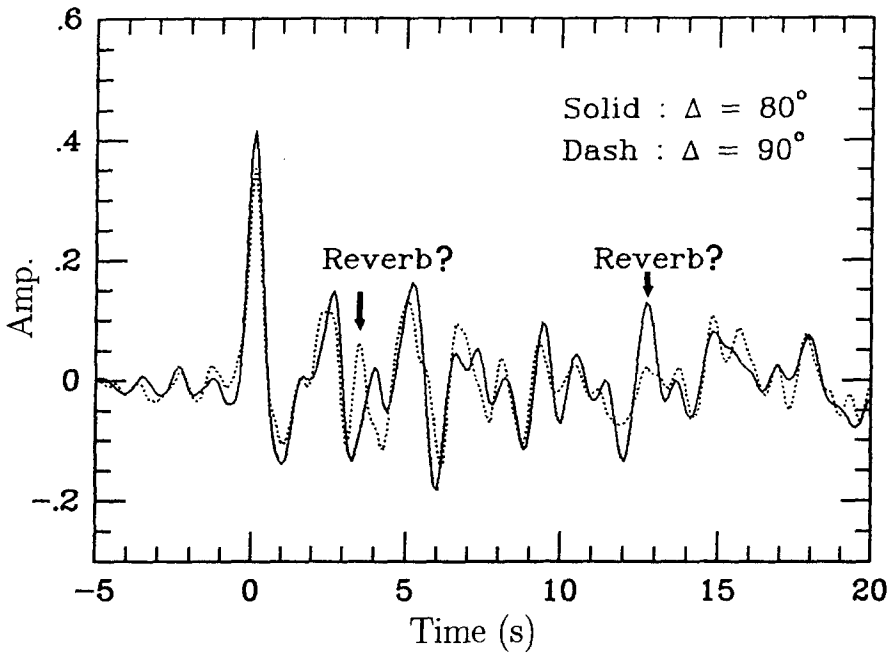

FIG. 7. Stacked radial receiver functions (data recorded at ALB-B) having a backazimuth of 230° but slightly different Δ's (80° and 90°). The two phases labeled "Reverb?" exhibit rapid amplitude and arrival-time variations and cannot be modeled as *Ps* conversions generated at a planar dipping interface. Stacking over narrow BAZ or Δ ranges allows the identification of such erratic phases that represent either reverberations or scattered energy.

Lateral Sampling Range of Ps and Reverberations

In many previous receiver function studies (e.g., Owens *et al.*, 1987), lateral variations in Earth structure were identified by developing different Earth models for arrivals from different backazimuths (e.g., NW, SE, SW). For dipping layers, an Earth model that satisfies the observed data from all backazimuths is sought. To ascertain the sampled region, the lateral range of both *Ps* phases and reverberations are examined. The reference model used in the following calculations is that given in Table 1 and arrivals from $\Delta = 80°$ ($p = 0.046$ sec/km) are considered. Although the exact lateral extent of sampling of *Ps* will be more complex than that illustrated by this simple model, experiments with more complicated models indicate that for *Ps* the ranges determined here are valid first-order estimates.

First, the lateral extent of sampling by *Ps* phases and reverberations on a horizontal interface at 60 km depth is examined. The four-layer Earth model of Table 1 (with all dip angles set to 0°) is considered. Figure 8b illustrates a simplified version of this model; only the boundary at 60 km depth is shown. In Figure 8a the solid circle of ~ 12 km radius centered on the recording site denotes the points at which *Ps* phases would be generated for *P* waves approaching from all azimuths. In fact, due to the finite bandwidth of the waves, this is a minimum estimate of the sampled area. The circle should be a finite radius ring having a width determined by the frequency of the wave and depth of the interface. For a 0.5-Hz plane *S* wave at 60 km depth the Fresnel zone width is approximately 25 km. The dotted circle of ~ 50 km radius

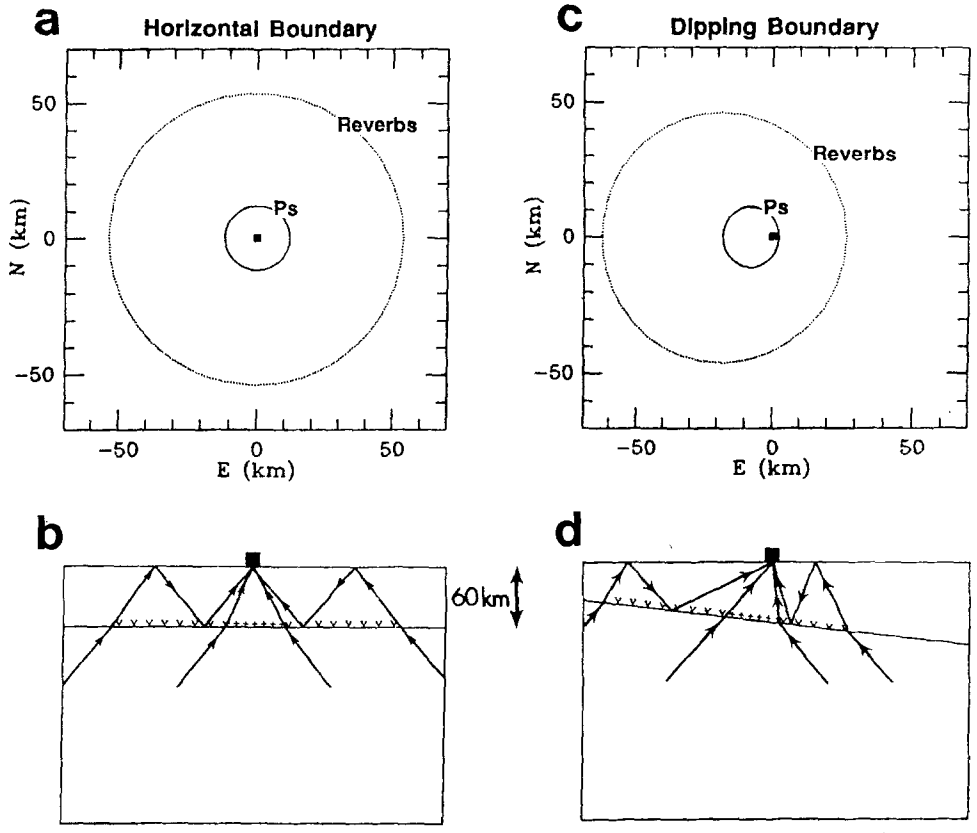

FIG. 8. Examples of the lateral extent of sampling provided by *Ps* conversions and reverberations in plan view (top) and cross section (*bottom*) for a horizontal boundary (*a*, *b*), and a dipping boundary (*c*, *d*). The cross section represents a simplified version of the four-layer Earth model used. For both cases, the boundary is at 60 km depth and arrivals from $\Delta = 80°$ are considered. Arrivals from a smaller Δ will sample a larger area (see text). In the case of a horizontal boundary, a circular area about the recording site (black square) is sampled; for a dipping boundary, the area sampled is offset to the updip side of the station.

denotes the approximate limit of the area sampled by reverberations. For dipping layers (using the model of Table 1), the lateral extent of sampling has shifted to the updip side of the station (Fig. 8c and d). Due to refraction of waves at a dipping boundary, arrivals approaching from the dip direction contain *Ps* phases generated very close to the recording site (2 km downdip). *Ps* arrivals from the opposite direction, however, were generated approximately 18 km updip of the recording station. Reverberations show a similar pattern but sample over larger distances. Those approaching from the dip direction were generated ~ 30 km downdip of the station, whereas those from the opposite BAZ were generated ~ 60 km updip of the recording station.

Thus, in the case of a boundary dipping 20° at 60 km depth, the *Ps* phases observed in receiver functions representing the updip and downdip directions were generated at points on the boundary approximately 20 km from one another (i.e., 4 to 5 seismic wavelengths). The planar boundary assumption used in modeling receiver functions is likely valid over this distance range. However, reverberations may be generated at points separated by 100 km or more (20 to 25 seismic wavelengths), and it is likely that the assumption of a

planar, dipping interface will begin to break down. As a result of this, it is doubtful that reverberations from deep dipping interfaces can successfully be modeled without considering lateral variations in the Earth structure.

This example considers a specific case of a boundary dipping 20° at 60 km depth and $\Delta = 80°$. For a smaller Δ, the sampling range of both *Ps* and reverberations will be greater and for a given Δ the lateral sampling range of all phases will be smaller for shallower boundaries and larger for deeper boundaries. In more general terms, for a horizontal boundary and a Δ range of 45° to 80° the total lateral sampling range of *Ps* will be ~ 0.4 to 0.7 times the depth of the generating boundary, while reverberations will sample a total lateral distance of 2 to 3 times the depth of the interface. For a boundary dipping ~ 20°, *Ps* and reverberations will sample a maximum lateral range of 0.3 to 0.5 times and 1.5 to 3 times the depth of the generating interface, respectively.

Thus, when modeling, one should consider the depth and dip angle of the boundary of interest and the frequency content of the data, estimate the total lateral sampling range of *Ps* and reverberations, and judge whether the planar boundary assumption is justifiable.

Stability of Reverberations

Shear-wave reverberations form an integral component of receiver functions. An incident *P* wave has the potential to generate numerous reverberatory phases (Fig. 9a) that arrive at times approximately 3 to 4 times greater than that of *Ps*. The top trace in Figure 9b illustrates *Ps* and reverberations contained in a radial receiver function generated using the very simple horizontal layered Earth model of Figure 9a. Note that two of the Moho reverberations, *PpPms* and *PpSms*, have an amplitude comparable to that of *Ps*. For a horizontal boundary, the amplitude and arrival time of *Ps* and all reverberations are independent of BAZ. In addition, *P*-wave reverberations (i.e., *PpPmp*) associated with horizontal interfaces arrive at the surface at the same angle of incidence as the direct *P* wave and are therefore removed from the receiver functions by source equalization (Langston, 1979).

To illustrate the effect of a dipping layer on reverberations (see also Langston, 1977b), consider the simple model shown in Figure 9a but with the Moho dipping 15° to the east. In this case *P*-wave reverberations arrive at the surface at a different angle of incidence than the direct *P* wave and therefore these phases are not completely removed by source equalization; the amount of *P* energy removed by this process is dependent upon the BAZ of wave approach (Ammon, 1985). Figure 9b (lower three traces) demonstrates the large variations in both the amplitude and arrival time of the reverberations that occur as a function of BAZ. Note that the phase *PpPmp*, which is observed in updip arrivals (positive polarity) and in downdip arrivals (negative polarity), is not present in the horizontally layered case. Also note that *PpPms* and *PpSms* exhibit drastic variations in amplitude, arrival time, and polarity as a function of BAZ. Significant variations in the amplitude and arrival time of reverberations may occur as a function of Δ (not shown). Note that *Ps* amplitudes always decrease for increasing Δ (or decreasing ray parameter; see Fig. 5). In contrast, the amplitude of reverberations may remain constant or even increase with increasing Δ. This may be useful to discriminate between reverberations and *Ps* conversions. Additionally, reverberations and scattered energy may be iden-

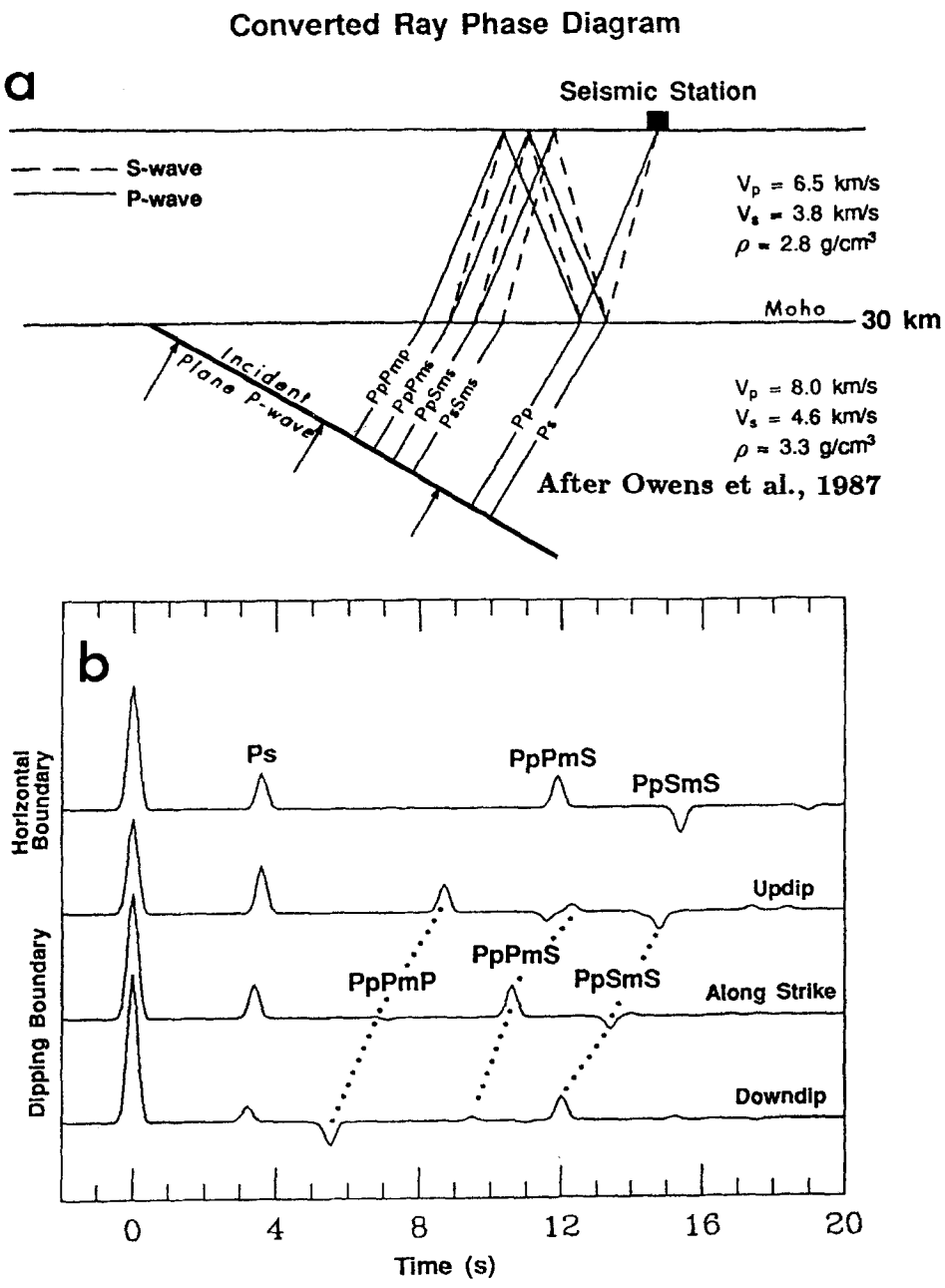

FIG. 9. (a) Simplified ray diagram illustrating the reverberations and conversions that may be generated by a *P*-wave incident at a boundary. (b) Corresponding receiver functions for the model shown assuming a horizontal boundary (top trace) and a boundary dipping 15° to the east (lower three traces). Technically, the *P* wave generates two to three reverberations with amplitudes comparable to the *Ps*. In the case of a dipping layer, drastic amplitude and arrival-time variations occur as a function of backazimuth (lower three traces).

tified by their rapid variations in either amplitude or arrival time over a small range of BAZ or Δ (as illustrated in Fig. 7).

Thus, for reverberations associated with dipping interfaces, the variation in the polarity, amplitude, and arrival time as a function of BAZ and Δ, and the

large lateral sampling area (relative to *Ps* phases), suggests that it would be extremely difficult to accurately model such phases. Formal inversion techniques, which attempt to match all arrivals in a waveform, must be applied with extreme caution. It would be prudent to begin by forward modeling only those phases whose amplitude and arrival time variations as a function of both BAZ and Δ are indicative of *Ps*. Then, only those portions of the receiver functions that are relatively free of reverberations could be inverted, or the inversions could be weighted to reduce the dependence on those segments of the receiver function suspected of containing reverberations or scattered energy.

Forward Modeling and the Resolution Capability of Receiver Functions

Most broadband receiver function studies have formally inverted radial receiver functions (e.g., Owens *et al.*, 1984) to estimate the fine-scale (1 to 2-km-thick layers) Earth structure. In the previous section, it was suggested that in a dipping layer environment only *Ps* phases should be modeled. Here, the resolution capability of receiver functions and the factors that should be considered when forward modeling are examined. Specifically, the minimum detectable ΔV_s, transition zones, and the "thinness" of a thin-layer that may be detected are examined.

Minimum Detectable ΔV_s

When forward modeling receiver functions, a valid question is: what is the minimum ΔV_s at a boundary that will generate an observable *Ps* phase in the waveform? This will depend upon the receiver function noise level and the amplitude of the *Ps* phase. The noise level is influenced by processing noise, Earth noise (e.g., microseisms) and the scattering level associated with both near-source and receiver structure. The scattering level is site dependent (e.g., see Langston, 1989; Langston and Ammon, 1991) and is not considered here; thus these minimum detectable ΔV_s estimates represent lower bounds. The amplitude of the *Ps* phase is dependent upon the angle of incidence at a boundary (Ammon, 1991). This is dependent upon Δ and, in the case of dipping layers, the backazimuth. Therefore, the data distribution will play a role in determining the minimum detectable ΔV_s.

Table 2 provides the amplitudes of *Ps* phases generated at horizontal interfaces having *S*-velocity contrasts of 0.10 to 0.50 km/sec for epicentral distances of 45° (p = 0.068) and 80° (p = 0.046). By considering the average noise level of the data set and the data distribution, it is possible to estimate the minimum detectable ΔV_s. For example, in a receiver function study in the Cascadia subduction zone (Cassidy and Ellis, 1991), the average noise level associated with the stacked receiver functions was approximately ± 0.04 P_z. Bold-faced values in Table 2 denote *Ps* amplitudes that are larger than this average noise

TABLE 2

Ps Amplitude as a Function of ΔV_S and Δ

	ΔVs (km/sec)							
Δ	0.10	0.20	0.25	0.30	0.35	0.40	0.45	0.50
45°	0.018	0.037	**0.046**	**0.055**	**0.064**	**0.074**	**0.083**	**0.092**
80°	0.011	0.022	0.027	0.032	0.038	**0.043**	**0.049**	**0.054**

level. In this study, approximately one half of the data set consisted of arrivals from $\Delta = 30°$ to $60°$ and one half consisted of arrivals from $\Delta = 70°$ to $100°$. Therefore, it was estimated that boundaries having an *S*-velocity contrast $\geqq 0.3$ km/sec could be resolved.

As demonstrated earlier, *Ps* amplitudes generated at a dipping interface vary as a function of BAZ. In the event of a very large azimuthal gap in the data set (i.e., $> 180°$), a dipping interface having a significant velocity contrast (e.g., $\Delta V_s \sim 0.5$ km/sec) could be missed if the data gap coincided with the dip direction of the boundary. Otherwise, the ability to resolve dipping interfaces should be similar to that for horizontal interfaces.

Transition Zones versus First-Order Velocity Discontinuities

To examine the ability to distinguish first-order velocity discontinuities from transition zones, experiments were performed using synthetic data and various Earth models. Figure 10 illustrates *Ps* conversions contained in radial receiver functions dominated by three frequency passbands: $a = 7$, 5, and 3 (for $f < 2$, 1, and 0.5 Hz, respectively). Each of the three series of traces compares a *Ps* conversion at a first-order velocity discontinuity (top trace) with those generated at a linear transition zone from 1 to 5 km thick (lower five traces). The *S*-velocity contrast is 0.58 km/sec. The numbers beside each *Ps* represent the amplitude of the conversion relative to one generated at a first-order velocity discontinuity. For an a value of 5.0, it is difficult to distinguish a discontinuity from a transition zone up to 2 km thick. Similarly, for an a value of 3.0, it is difficult to distinguish a discontinuity from a transition zone up to ~ 3 km

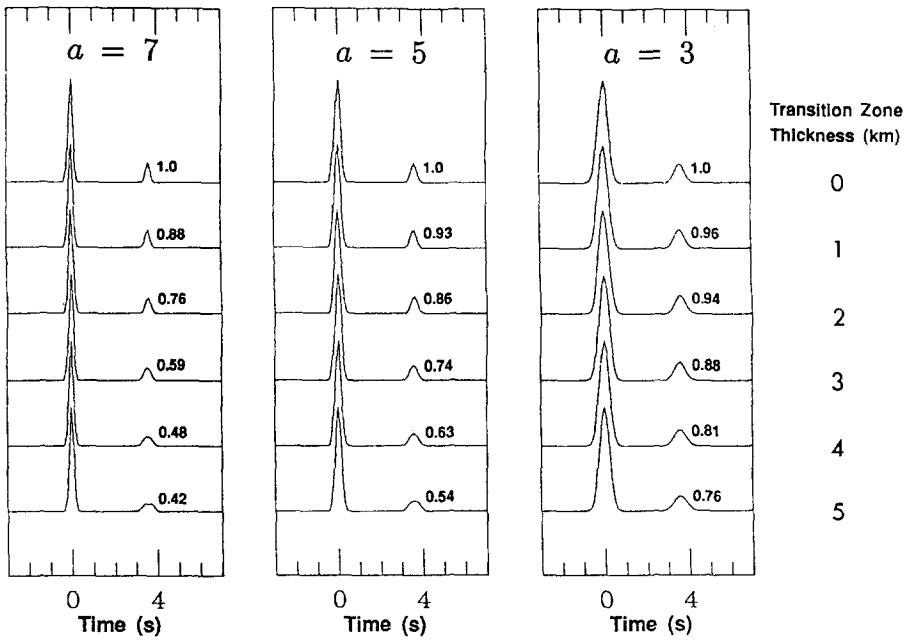

FIG. 10. Resolution of 1- to 5-km-thick transition zones provided by the three frequency passbands represented by $a = 7$, $a = 5$, and $a = 3$ (see text). The numbers beside each *Ps* phase represent the amplitude relative to a *Ps* phase generated at a first-order velocity discontinuity (top trace in each case).

thick. However, it should be noted that in the presence of noise the resolving power will be reduced. Broad transition zones (thicker than ~ 3 km) could be identified using broadband data by comparing receiver functions generated with different a values (Ammon, 1985; Owens and Zandt, 1985). For example, a transition zone 5 km thick may be identified by an approximate doubling of the *Ps* amplitude for $a = 3$ relative to $a = 7$ (Fig. 10).

Resolution of Thin Layers

The ability to discriminate thin layers represents a dramatic improvement of broadband receiver function studies over previous long-period studies that could only provide details on gross crustal properties. Using synthetic data, the "thinness" of thin layers that may be resolved with this technique is examined. Figure 11 illustrates the ability of the three frequency passbands represented by $a = 7$, 5, and 3 to resolve a "thin" low S-velocity layer (ranging from 1 to 5 km thick). Note the top trace was calculated using a 10-km-thick layer; the amplitude of this *Ps* phase is the reference value against which the others are compared. The model has a thin layer of $V_s = 3.47$ km/sec embedded in a region of $V_s = 4.05$ km/sec.

The highest-frequency receiver functions ($a = 7$) successfully resolve layers as thin as 1 to 2 km; for $a = 5$, layers as thin as 2 to 3 km may be resolved; and for the lower frequency events ($a = 3$), layers 4 to 5 km thick may be resolved without a significant loss of information ($\leq$ 10% *Ps* amplitude decrease). Attempting to resolve a thinner layer than is justified by the frequency content of

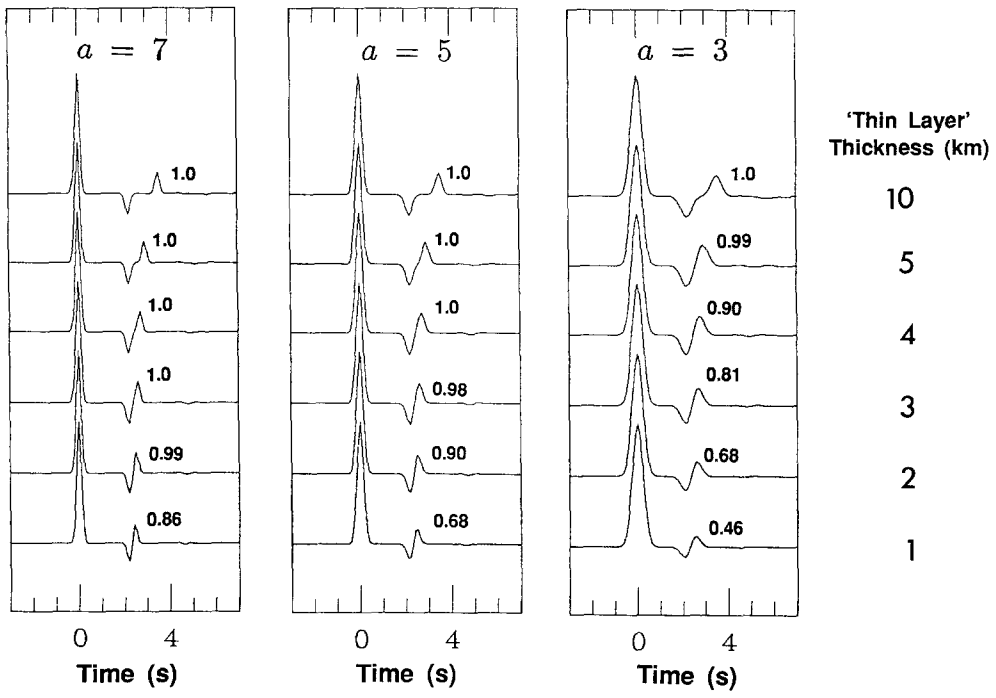

FIG. 11. Resolution of a thin layer (1- to 5-km thickness) provided by the three frequency passbands represented by $a = 7$, 5, and 3. The numbers beside each *Ps* phase are the amplitude relative to a *Ps* phase generated at a 10-km-thick layer (top trace).

the data would result in an underestimate for the ΔV_s of the low-velocity zone. It should be noted that all synthetic receiver functions were generated using a Gaussian pulse (having a width controlled by a) convolved with a spike series. For real data, the ability to resolve thin layers will be reduced by noise. Also, if the averaging function is not a simple Gaussian or delta-like pulse, a loss of resolution will result. This is discussed further in the next section.

Choice of A Forward Modeling Time Function

The frequency-dependent response of receiver functions illustrated above does not pose a problem in modeling but rather provides an opportunity to identify and examine features such as thin layers and broad transition zones by considering different frequency bands of data. The examples above indicate the importance of matching the frequency content of synthetic receiver functions to that of the observed data. This is best achieved by choosing a Gaussian time-function that has a half-width (controlled by the a value in equation 4) comparable to that of the direct P wave on the observed radial receiver function.

The resolving power of a receiver function may be examined by estimating, using equation (3), the averaging function, $A(\omega)$, associated with the deconvolution. If it is not a simple, Gaussian-like pulse, but rather contains significant side-lobes it could be used in the forward modeling stage to generate synthetic receiver functions more appropriate for matching the observed data.

Conclusions

In this paper, a series of numerical experiments were performed to examine several important aspects of receiver function analysis, with emphasis on applications to the study of dipping interfaces. The recent modification introduced to the receiver function analysis technique that preserves absolute amplitude information (Ammon, 1991) is shown to be more robust than the previous technique of modeling relative amplitudes. It is demonstrated that shallow (depth less than ~ 2 km) high-velocity contrast interfaces, which may be difficult to detect, can alter the relative amplitudes of Ps phases (Ps/P_r) generated at deeper boundaries. Thus, modeling relative amplitudes may result in inaccurate Earth models. However, modeling absolute amplitude receiver functions minimizes this potential for error.

If research targets include deep dipping structure, tight stacking bounds ($\leqq 10^\circ$ in both Δ and BAZ) should be applied. There are advantages to stacking over a narrow range of BAZ and Δ, including the ability to identify those phases exhibiting rapid variations in either amplitude or arrival time as a function of BAZ or Δ. Such phases are likely reverberations or scattered energy.

Reverberations sample an area of radius ~ 1 to 1.5 times the depth of the reflecting interface. For deep boundaries (e.g., 50 to 60 km depth), the total lateral extent of sampling by reverberations is ~ 100 to 180 km. Undoubtedly, the modeling assumption of planar boundaries will be invalid over such distances in a complex tectonic setting. Reverberations associated with dipping interfaces will be difficult to identify due to their drastic variations in arrival time and amplitude as a function of BAZ and Δ. Thus, they cannot readily be used to provide constraints on Earth structure. As reverberations are an important constituent of receiver functions, formal inversion techniques must be applied with caution to data collected in complex tectonic settings.

When forward modeling receiver functions, the minimum detectable ΔV_s should be within the range 0.2 to 0.4 km/sec, depending upon the average noise level of the data set and the data distribution. Broadband receiver functions have the potential to resolve layers of 2 to 5 km thickness. Transition zones may be examined by considering various frequency bands of the data. The resolving power of receiver functions may be examined by computing the averaging functions associated with the deconvolutions. If significant sidelobes are observed, the averaging function could be used in the forward modeling stage to provide for a better comparison of observed and synthetic data.

Acknowledgments

I wish to thank Robert M. Ellis for critically reviewing this manuscript and his advice during the course of this research. Thanks also go to Doug Oldenburg for enlightening discussions on deconvolutions and averaging functions. The contribution of analysis programs of Thomas J. Owens and helpful reviews by Charles Ammon and George Zandt are gratefully acknowledged. Funding for this program has been provided by Energy, Mines and Resources Canada Research Agreement 89-84, the Natural Science and Engineering Research Council of Canada Grant A2617, and the British Columbia Hydro and Power Authority. The author was partially supported by a University Graduate Fellowship.

References

Ammon, C. J. (1985). Time domain teleseismic P waveform modeling and the crust and upper mantle structure beneath Berkeley, California, *M.S. Thesis*, State University of New York, Binghamton, 97 pp.

Ammon, C. J. (1991). The isolation of receiver effects from teleseismic *P* waveforms, *Bull. Seism. Soc. Am.* **81**, 2504-2510.

Ammon, C. J., G. E. Randall, and G. Zandt (1990). On the nonuniqueness of receiver function inversions, *J. Geophys. Res.* **95**, 15,303-15,318.

Burdick, L. J. and C. A. Langston (1977). Modeling crustal-structure through the use of converted phases in teleseismic body-waveforms, *Bull. Seism. Soc. Am.* **67**, 677-691.

Cassidy, J. F. (1991). Teleseismic receiver function analysis of the crust and upper mantle of southwestern British Columbia, *Ph.D. Thesis*, University of British Columbia, Vancouver, B.C., 174 pp.

Cassidy, J. F. and R. M. Ellis (1991). Shear wave constraints on a deep crustal reflective zone beneath Vancouver Island, *J. Geophys. Res.* **96**, 19,843-19,851.

Clayton, R. W. and R. A. Wiggins (1976). Source shape estimation and deconvolution of teleseismic body waves, *Geophys. J. R. Astr. Soc.* **47**, 151-177.

Langston, C. A. (1977a). Corvallis, Oregon, crustal and upper mantle structure from teleseismic *P* and *S* waves, *Bull. Seism. Soc. Am.* **67**, 713-724.

Langston, C. A. (1977b). The effect of planar dipping structure on source and receiver responses for constant ray parameter, *Bull. Seism. Soc. Am.* **67**, 1029-1050.

Langston, C. A. (1979). Structure under Mount Rainier, Washington, inferred from teleseismic body waves, *J. Geophys. Res.* **84**, 4749-4762.

Langston, C. A. (1989). Scattering of teleseismic body waves under Pasadena, California, *J. Geophys. Res.* **94**, 1935-1951.

Langston, C. A. and C. J. Ammon (1991). Scattering of teleseismic body waves along the Hayward-Calaveras fault system, *Bull. Seism. Soc. Am.* **81**, 576-591.

Lapp, D. B., R. S. Crosson, and T. J. Owens (1990). P-waveform analysis for local subduction geometry south of Puget Sound, Washington, *Pure App. Geophys.* **133**, 349-365.

Owens, T. J. (1984) Determination of crustal and upper mantle structure from analysis of broadband teleseismic P-waveforms, *Ph.D. Thesis*, University of Utah, Salt Lake City, 146 pp.

Owens, T. J. and R. S. Crosson (1988). Shallow structure effects on broadband teleseismic *P* waveforms, *Bull. Seism. Soc. Am.* **78**, 96-108.

Owens, T. J., R. S. Crosson, and M. A. Hendrickson (1988). Constraints on the subduction geometry beneath western Washington from broadband teleseismic waveform modeling, *Bull. Seism. Soc. Am.* **78**, 1319-1334.

Owens, T. J., S. R. Taylor, and G. Zandt (1987). Crustal structure at regional seismic test network stations determined from inversion of broadband teleseismic *P* waveforms, *Bull. Seism. Soc. Am.* **77**, 631-662.

Owens, T. J. and G. Zandt (1985). The response of the continental crust-mantle boundary observed on broadband teleseismic receiver functions, *Geophys. Res. Lett.* **12**, 705-708.

Owens, T. J., G. Zandt, and S. R. Taylor (1984). Seismic evidence for an ancient rift beneath the Cumberland Plateau, Tennessee: a detailed analysis of broadband teleseismic P waveforms, *J. Geophys. Res.* **89**, 7783-7795.

Phinney, R. A. (1964). Structure of the Earth's crust from spectral behaviour of long-period body waves, *J. Geophys. Res.* **69**, 2997-3107.

Department of Geophysics and Astronomy
University of British Columbia
2219 Main Mall
Vancouver, British Columbia
Canada V6T 1Z4

Manuscript received 4 June 1991